Research Article

Journal of RAMAN SPECTROSCOPY

Received: 3 April 2009 Accepted: 15 May 2009 Published online in Wiley Interscience:

(www.interscience.wiley.com) DOI 10.1002/jrs.2392

A high-throughput method for controlled hot-spot fabrication in SERS-active gold nanoparticle dimer arrays

Kristen D. Alexander,[a]* Meredith J. Hampton,[b] Shunping Zhang,[c] Anuj Dhawan,[d] Hongxing Xu,[c] and Rene Lopez[a]

We present a high-throughput method for fabricating large arrays of surface-enhanced Raman scattering (SERS) active gold dimers. Using a large-area/low-cost nanopatterning method in conjunction with a meniscus force deposition technique, we were able to create large arrays of uniformly spaced nanoclusters comprising two 60-nm gold nanospheres. Raman measurements of a thiophenol monolayer deposited on smaller scale arrays of aligned dimers yielded enhancement factors as high as 10^9. Polarization-controlled measurements show spectral peak heights to be 10–100 times smaller when the incident beam is polarized perpendicularly to the dimer axis, confirming that the measured enhancements arise from the 'hot spots' between the two nanospheres.

Keywords: surface-enhanced Raman scattering (SERS); gold nanoparticles; hot spot; enhancement factor; templating

Introduction

The ability to detect and identify substances efficiently is of great scientific interest. This is a task for which Raman spectroscopy is well suited. However, trace Raman detection has proven difficult to achieve due to the limitations imposed by its small scattering cross section.[1] In 1977, small analyte detection started to become possible thanks to enhancements originating from molecules in the proximity of roughened metallic surfaces.[2] This effect, known as surface-enhanced Raman scattering (SERS), has been suggested to be capable of single-molecule detection.[3–5] The emergence of SERS presented an avenue around intrinsic signal strength problems and has renewed interest in Raman spectroscopy for a wide range of applications.[6–8] However, while significant progress has been made toward Raman detection of very dilute analytes, the technique is still limited due to the unreliable reproducibility of large enhancement factors.[9,10]

The lack of reproducibility of enhancement factors is not surprising since the regions where enhancements are particularly large (i.e. 'hot spots') are commonly limited to the few cubic nanometers of volume between adjacent nanoparticles.[11] Furthermore, several studies have shown that these enhancements are extraordinarily sensitive to nanocluster morphology, the wavelength and polarization of the excitation source, and, perhaps above all, the interparticle spacing and the resultant plasmon coupling coupling.[11–20] Although many of these studies have carried out theoretical simulations to predict the electric field enhancements arising from various types of nanoclusters, there have been few successful attempts to tease out these behaviors from real nanoscopic features since a reliable method for their timely fabrication and systematic testing remained elusive. Advances in electron and ion beam lithography have made it possible to control the morphology and location of particles down to a few nanometers, but such precision is still insufficient to test these effects. On the other hand, other groups have succeeded in linking gold nanoparticles in a controlled manner to create small clusters with known interparticle spacing[21,22] but the process is low throughput and, more importantly, produces random cluster orientations that obscure the characterization process.

In this paper, we experimentally address these theoretical predictions by making measurements of the enhancement factors produced by clusters of a specific size and morphology. Recognizing that the key to characterization of this effect lies in the ability to produce large quantities of nearly identical clusters, we approach this problem using a technique that deftly exploits the advantages of parallel fabrication. We direct metal nanoparticles to form large, ordered arrays of only dimers with controlled size, orientation, and placement with respect to fiducial patterns. Here, we are able to demonstrate the degree of dependence of the SERS enhancement factor on different parameters. Specifically, we measured a 10^9 enhancement factor for two closely spaced 60-nm gold nanospheres with a marked sensitivity to the polarization angle with respect to the dimer axis.

* *Correspondence to: Kristen D. Alexander, Department of Physics and Astronomy, University of North Carolina, Chapel Hill, NC, USA. E-mail: krisalex@physics.unc.edu*

a *Department of Physics and Astronomy, University of North Carolina, Chapel Hill, NC, USA*

b *Department of Chemistry, University of North Carolina, Chapel Hill, NC, USA*

c *Institute of Physics, Chinese Academy of Sciences, Beijing 100080, P. R. China*

d *Department of Biomedical Engineering, Duke University, Durham, NC, USA*

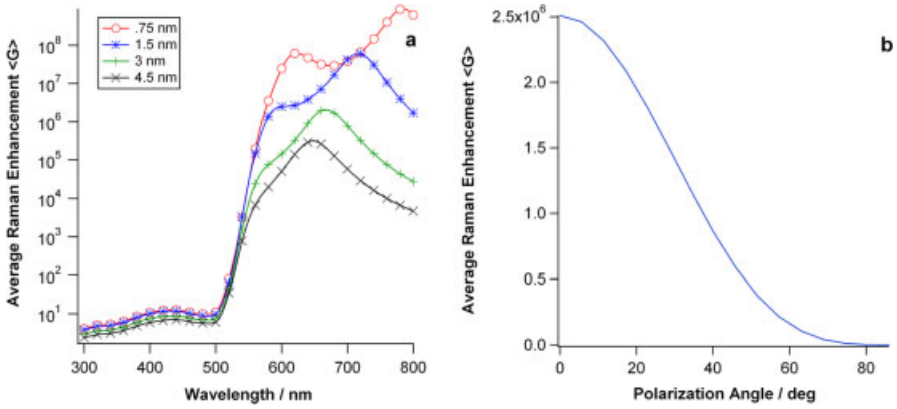

Figure 1. (a) Surface-averaged Raman enhancement over the surface of two 60-nm gold spheres over a range of spacings. Projected Raman enhancement would go roughly as the square of the field intensity. (b) Raman enhancement factor as a function of incident polarization for two 60-nm gold spheres separated by 1.5 nm and illuminated with light of wavelength $\lambda = 632.8$ nm. The refractive index for the surrounding medium in both calculations is set at $n = 1.5$.

Experimental

Generalized Mie theory simulations

A strong polarization dependence is the clearest indication of an active hot spot. This is rooted in the fact that when metal nanoparticles are brought close together and illuminated with light of the correct wavelength, the resulting plasmon dipole modes can couple via near-field interaction. This coupling gives rise to SERS enhancements which peak in the hot spot when the excitation source is polarized parallel to the dimer axis and, likewise, reaches a minimum when the polarization is rotated 90°. To illustrate this, we have carried out generalized Mie theory simulations[23–25] for the electromagnetic enhancement in the area immediately around two gold nanoparticles. The Raman enhancement can rigorously be shown to be proportional to the product of the squares of the field enhancement factors at the incident and Raman frequencies $G = |f(\omega_{\text{Raman}})|^2 |f(\omega)|^2$. Provided that $|\omega_{\text{Raman}} \pm \omega|$ is smaller than the spectral response of the metal nanostructure, the Raman scattering enhancement scales roughly with the fourth power of the electric field enhancement:

$$G(\mathbf{r}) \approx \frac{|E_{\text{loc}}(\mathbf{r})|^4}{|E_0(\mathbf{r})|^4} \tag{1}$$

Since the molecular species to be detected could be located anywhere close to the metal surface, the Raman enhancement factor must be averaged over the entire cluster surface:

$$\langle G(\mathbf{r}) \rangle = \frac{1}{\sum_i^2 4\pi R_i^2} \sum_i^2 \int_i G(\mathbf{r}) d\sigma \tag{2}$$

where R is the metal nanoparticle radius and the sum is carried out to two to account for the individual spheres that make up the dimer.

Our simulation comprises two nanospheres 60 nm in diameter separated by an interstitial gap ranging from 0.75 to 4 nm. In the case of parallel polarization, the total Raman enhancement is shown to be strongly dependent on the separation of the particles and the excitation wavelength (Fig. 1(a)): enhancements, blue shift, and decrease at a staggering rate of approximately one order of magnitude per nanometer of separation. Conversely, the total Raman enhancement factor is shown to drop off dramatically as the polarization angle with the dimer axis increases, bottoming out at levels analogous to that of an uncoupled nanoparticle (Fig. 1(b)). For the dimer, this polarization sensitivity is a crucial characteristic of the hot spot since this relationship weakens with increasing interparticle gap.

Array fabrication

A combination of chemical and physical methods to control different length scales has enabled us to experimentally confront the simulation predictions. Nanolithography tools are used to make a template to control scales in the 100-nm range, while molecular spacers are used to modify and hold the spacing between nanoparticles. The process we present here serves to create localized dimers as well as place them in large-scale arrays.

Large-scale nanoparticle placement is facilitated by the use of a grid of nanoholes in a silicon substrate. This structure is fabricated by applying current advances in low-cost/large-area nanofabrication pioneered by the DeSimone group at University of North Carolina (UNC).[26,27] This soft lithography technique, known as PRINT™ for Pattern Replication in Nonwetting Templates, utilizes a low-surface-energy perfluoropolyether (PFPE) polymer. PFPE elastomers as a molding material are unique with respect to their silicone-based counterparts because their very low surface energy, inertness, and tunability permit them to pattern large arrays of sub-100-nm features that can be easily separated from the mold. To create our templates, an array of 200-nm wide by 600-nm high poly(lactic-co-glycolic acid) (PLGA) round-based posts is deposited over a 100-nm-thick 'flash' layer on a silicon wafer coated in 300 nm of SiO_2. The wafer is then placed in a reactive ion etcher and directionally etched for 45 s to remove the flash layer. Next, 20 nm of Cr is deposited on the posts by electron beam evaporation. After the Cr deposition is complete, the sample is sonicated in acetone for 60 min to remove the PLGA posts and expose the SiO_2 originally masked by the polymer, creating an array of circles masked by Cr. The sample is then placed in the reactive ion etcher and etched for 90 s to create 100-nm deep pits in the unmasked SiO_2. Once the dry etch is complete, the Cr mask is removed using CR-14 chrome etch (Transene) and then rinsed in a 2% sulfuric acid solution to remove precipitates from the chrome

Journal of RAMAN SPECTROSCOPY

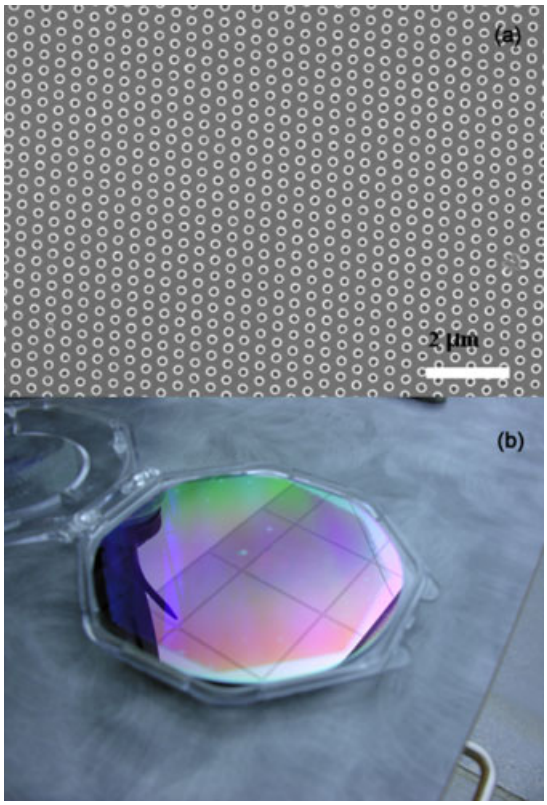

Figure 2. (a) Scanning electron micrograph of an array of nanoholes patterned into a silicon wafer after Cr deposition, removal of PLGA posts, and reactive ion etching. (b) Aspect of whole wafer patterned with nanoholes.

etchant. Atomic force microscope measurements confirm the final product as an array of 120-nm wide by 100-nm deep holes with a center-to-center spacing of 350 nm (Fig. 2).

The nanoparticles are positioned in the hole arrays by a meniscus force deposition method.[28] To achieve this, a piece of nanopatterned substrate is subjected to a brief plasma treatment to make the SiO_2 hydrophilic and then immersed in an aqueous gold nanoparticle colloid and allowed to evaporate in a temperature-controlled environment. As the meniscus slowly recedes across the substrate, nanoparticles concentrate at the three-phase contact line (Fig. 3(a)). Because the 120-nm diameter holes can hold only two nanoparticles, several large areas of our substrate contain mostly dimers when the process is complete. Finally, individual dimers were identified on the silicon substrate via electron microscope imaging (Fig. 3(b)). Note that the dimers in Fig. 3(b) are randomly oriented within the wells (the original master was composed of circular cylinders and was not intended for this application). Dimer orientation cannot be determined optically for this particular sample, making it difficult to verify the accuracy of on- and off-axis polarization measurements. In order to more precisely position nanoparticle pairs, we used focused ion beam (FIB) milling to fabricate a master template of rectangular wells tailored to the dimensions of the dimers (Fig. 3(c)). These wells provide greater spatial constraint for the nanoparticles, which forces the dimers into a definite orientation.

When nanoparticles are initially deposited from the gold colloid, they are encased in a monolayer of sodium citrate. In solution, the citrate molecule acts a surfactant, keeping the nanoparticles from aggregating. When they are deposited in the wells, however,

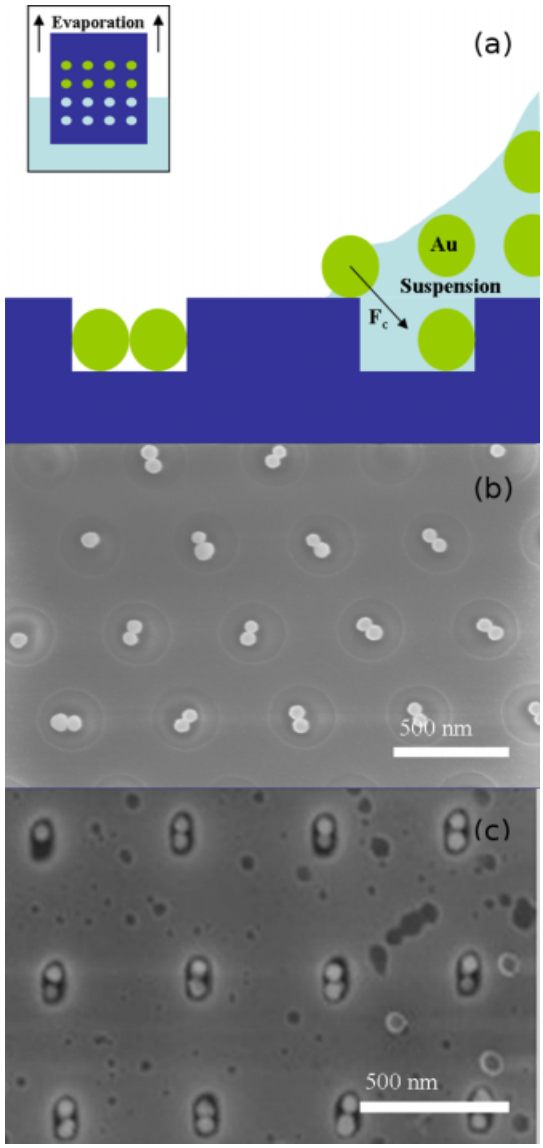

Figure 3. (a) Schematic illustrating the capillary force (F_c) assembly mechanism at the vapor–suspension–substrate three-phase contact line. (Inset) Movement of the three-phase contact line driven by evaporation by heating the solution to 60 °C per Ref. [28], (b) gold dimer array fabricated by a combination of pattern replication, wafer processing techniques, and solvent evaporation, (c) gold dimer array fabricated by focused ion beam milling and solvent evaporation.

the citrate molecules act as spacers, preventing the gold surfaces from touching each other. In order to both control and modify the spacing between nanoparticles, the citrate molecule must be replaced with another rigid molecule. We chose to use thiophenol because the high gold affinity of the SH end groups allows the molecule to easily displace the citrate. Additionally, thiophenol contains a benzene ring which has a large Raman cross section, making it easy to detect in low concentrations, and its length (~4.6Å, estimated using ChemDraw) is slightly less than that of a citrate molecule (~7.2 Å), making its placement between two closely spaced nanospheres plausible.

The arrays were immersed in a 0.1 mM solution of thiophenol in ethanol for 24 h in order to form a monolayer on the gold surface. When the substrate was removed and allowed to dry, the effects

of the evaporation pull the nanoparticles together, presumably leaving many dimers with several thiophenol molecules serving as spacing agents in the interstitial gap. Direct measurement via electron imaging of this spacing was intentionally avoided to prevent potentially deleterious effects on the integrity of the sample. The presence of the thiol in the hot spot was confirmed, however, by subsequent Raman measurements and demonstration of polarization dependence. Raman spectra of individual dimers were taken using a modified confocal microscope outfitted with a flat scanning stage (Nanonics) and connected to a linearly polarized 500 : 1 (632.8 nm) continuous wave (cw) He–Ne laser via a polarization preserving, single-mode fiber optic cable. In the microscope, the beam undergoes a collimated path and passes through a high-quality line filter and a $\lambda/2$ wave plate which is used to rotate the beam polarization. The laser is directed to the 150× microscope objective by a beam-splitting cube which also redirects the collected Raman signal to pass a Raman edge filter prior to being collected by a 100-μm multimode fiber and transmitted to a spectrometer equipped with a low-noise charge-coupled device (CCD) detector. All optics, including the beam-splitting cube, collimators, fiber optics, line and edge filters, and lenses inside the microscope are nonpolarizing. Power delivered to the sample across all polarizations was confirmed to be uniform within a 3% margin. A diffraction-limited 300-nm laser spot size was verified by imaging calibration grids of feature size above, below, and at the 300-nm limit. Preliminary tests indicate that, without sufficient filtering, persistent exposure to the laser beam causes the thiophenol monolayer, and consequently the Raman signal, to rapidly degrade. The avoid thermal ablation of the monolayer over the several measurements taken of each dimer to confirm the polarization dependence, we monitored the stability of the Raman signal over a range of beam powers and exposure times. These tests determined that the combination of a 65-μW laser power delivered on the sample with a 5-min acquisition time yielded sufficiently clear and stable spectra.

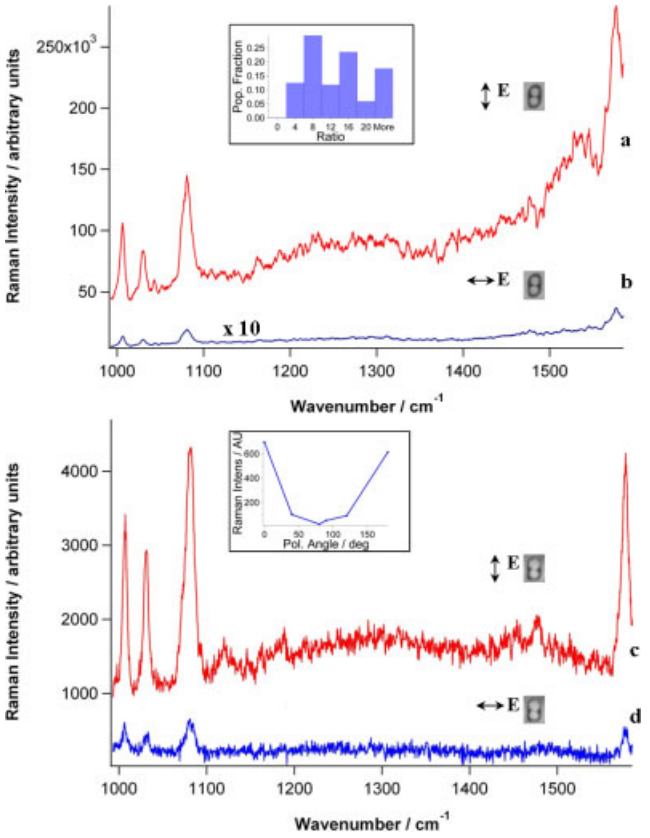

Figure 4. Thiophenol Raman lines measured from a single gold dimer with incident light polarizations (a), (c) parallel and (b), (d) perpendicular to the dimer axis. Traces (a) and (b) in the upper plot are representative of the largest enhancements we achieved in this experiment. The inset in this plot is a histogram showing the relative distribution of enhancement ratios between parallel and cross-axial polarization measurements, the largest of which was 79. Traces (c) and (d) in the lower plot are examples of what we typically measured in our polarization studies. The inset shows how the Raman intensity of an individual dimer varies as a function of polarization.

Results and Discussion

Raman spectra of gold dimers were taken while varying the polarization of the incident beam through a range of 90° relative to the dimer axis. Because the orientation of the dimers is predetermined, measurements through this full range were performed only for a small number of clusters. Most of the dimers were measured within a 10° range around the two dimer axes.

In this study we found that peaks measured when the incident beam was polarized in the parallel orientation were nearly 2 orders of magnitude taller than those peaks measured when the beam was polarized in the perpendicular orientation in the best cases (Fig. 4). Here, it is important to note that from the large number of dimers measured (50) the mode value of the polarization contrast was approximately a factor of 15 (see inset, Fig. 4). We attribute this to small variations of the dimer alignment in the wells, variations in nanoparticle size and morphology, and possibly the actual size of the interstitial gap, all of which, according to previous studies,[11–20] have strong effects on the enhancement factor. In particular, we note the possibility that the thiophenol molecules do not form a perfect monolayer on the gold surface in the vicinity of the hot spot. If too few or too many molecules assemble in the area, the interparticle spacing can be altered, drastically affecting the size of the enhancement factor. Nevertheless, the polarization contrast supports that hot spots do exist between these nanoparticles.

Additionally, the peak heights in the cross-polarization measurements were within a factor of 2 of the peak heights for isolated nanoparticles. This confirms, along with polarization contrast data, that most of the enhanced Raman signal comes from a small and highly localized area. By calculating this small area and attributing the difference in Raman signal between the two polarization states to the few molecules located there, we were able to estimate the enhancement factor for the hot spot. Specifically, we measured the Raman signal from bulk thiophenol in a solution of known concentration and compared the per-molecule signal strength with the per-molecule signal strength at the hot spot. The enhanced signal was assumed to arise entirely from an area spanning $\Omega = 2.4 \times 10^{-2}$ steradian spherical cap (a cone with 10° planar projection determined from simulation data) on each of the two nanoparticles. The surface enhancement factor (G) is defined as the ratio of the per-molecule enhancement from this spherical cap to the per-molecule enhancement from bulk thiophenol. Thus

$$G = \frac{I_{surf}/N_{surf}}{I_{bulk}/N_{bulk}} \tag{3}$$

N_{surf} is equal to the number of molecules occupying the area subtended by Ω multiplied by the molecular surface packing density of thiophenol and N_A Avogadro's number. In this

calculation, we used the value of 1.1 nmol cm^{-2}, the largest packing density currently reported in the literature.[29,30] N_{bulk} is defined as follows:

$$N_{bulk} = \pi r^2 hcN_A, \quad (4)$$

where r is the radius of the laser spot (150 nm), c is the molar concentration of pure thiophenol (9.77×10^{-3} mol cm^{-3}), and h is the effective focal depth of the objective (1 μm – determined by moving the objective above and below the focal point until the Raman signal disappears). Using this formula, the number of thiophenol molecules in the probe volume was estimated to be $N_{bulk} = 4.16 \times 10^8$.

The ratio of I_{surf}/I_{bulk} was taken on the 1575 cm^{-1} band. After removing the counts from the cross-polarization measurement to approximately separate the central hot spot Raman signal, the ratio was 1397 in the best sample and ≈200 in more typical cases. Both of these values were used to calculate SERS enhancement factors. Ultimately, we arrived at a range of 10^8–10^9 for the enhancement factor relative to the signal from bulk thiophenol. For cross-polarization measurements, the enhancement factor resulted in 10^3–10^4 and was calculated in the same way but under the assumption that all the thiophenol molecules coating the dimer surface contribute in equal proportion to the Raman signal. These measurements compare well with those of single gold nanoparticles,[11,19] and confirm that the multiparticle enhancement is not simply the sum of individual particle contributions.

Finally, we note that this technique lends an enormous amount of versatility to this study. Gold nanoparticles can be removed from substrates by treatment with aqua regia, so a single sample can be reused repeatedly. Moreover, while thiophenol was used in this experiment, molecular linkers of different sizes would add a greater degree of certainty to the gap size and could be used to achieve a wide range of interparticle spacings. Finally, features of virtually any size and shape down to 80 nm can be patterned into these substrates, allowing the fabrication of more complex clusters and arrays. Simulations performed in a recent study indicate that chains of several nanospheres can produce enhancement factors greater than those observed from dimers[31]; this technique offers a platform by which this theory can be tested.

Conclusions

We have demonstrated an inexpensive and reproducible method for the fabrication of large-scale nanopatterns in SiO_2. Using these templates, together with a meniscus force deposition method and molecular spacers, we were able to construct arrays of regularly spaced nanoclusters with a small interstitial gap. Subsequent Raman measurements made on well-aligned individual dimers demonstrated enhancement factors as large as 10^9 and polarization dependence consistent with the existence of SERS hot spots.

References

[1] M. Moskovits, *J. Raman Spectrosc.* **2005**, *36*, 485.
[2] D. L. Jeanmaire, R. P. Vanduyne, *J. Electroanal. Chem.* **1977**, *84*, 1.
[3] K. Kneipp, Y. Wang, H. Kneipp, L. T. Perelman, I. Itzkan, R. Dasari, M. S. Feld, *Phys. Rev. Lett.* **1997**, *78*, 1667.
[4] K. Kneipp, H. Kneipp, R. Manoharan, E. B. Hanlon, I. Itzkan, R. R. Dasari, M. S. Feld, *Appl. Spectrosc.* **1998**, *52*, 1493.
[5] S. M. Nie, S. R. Emery, *Science* **1997**, *275*, 1102.
[6] H. W. Liao, C. L. Nehl, J. H. Hafner, *Nanomedicine* **2006**, *1*, 201.
[7] N. Stone, M. C. H. Prieto, P. Crow, J. Uff, A. W. Ritchie, *Anal. Bioanal. Chem.* **2007**, *387*, 1657.
[8] J. Zhao, W. L. Qiu, D. M. Simeone, D. M. Lubman, *J. Proteome Res.* **2007**, *6*, 1126.
[9] P. G. Etchegoin, E. C. Le Ru, *Phys. Chem. Chem. Phys.* **2008**, *10*, 6079.
[10] N. P. W. Pieczonka, R. F. Aroca, *Chem. Soc. Rev.* **2008**, *37*, 946.
[11] J. Jiang, K. Bosnick, M. Maillard, L. Brus, *J. Phys. Chem. A* **2003**, *107*, 9964.
[12] E. Hao, G. C. Schatz, *J. Chem. Phys.* **2004**, *120*, 357.
[13] K. L. Kelly, E. Coronado, L. L. Zhao, G. C. Schatz, *J. Phys. Chem. A* **2003**, *107*, 668.
[14] K. H. Su, Q. H. Wei, X. Zhang, J. J. Mock, D. R. Smith, S. Schultz, *Nano Lett.* **2003**, *3*, 1087.
[15] M. Futamata, Y. Maruyama, M. Ishikawa, *J. Phys. Chem. A* **2003**, *107*, 7607.
[16] S. Foteinopoulou, J. P. Vigneron, C. Vandenbem, *Opt. Express* **2007**, *15*, 4253.
[17] L. Gunnarsson, E. J. Bjerneld, H. Xu, S. Petronis, B. Kasemo, M. Kall, *Appl. Phys. Lett.* **2001**, *78*, 802.
[18] H. X. Xu, J. Aizpurua, M. Kall, P. Apell, *Phys. Rev. E* **2000**, *62*, 4318.
[19] L. Gunnarsson, T. Rindzevicius, J. Prikulis, B. Kasemo, M. Kall, S. L. Zou, G. C. Schatz, *J. Phys. Chem. A* **2005**, *109*, 1079.
[20] M. Quinten, *Appl. Phys B* **2001**, *73*, 245.
[21] R. Sardar, T. B. Heap, J. S. Shumaker-Parry, *J. Am. Chem. Soc.* **2007**, *129*, 5356.
[22] L. C. Brousseau, J. P. Novak, S. M. Marinakos, D. L. Feldheim, *Adv. Mater. (Weinheim, Ger.)* **1999**, *11*, 447.
[23] Z. P. Li, H. X. Xu, *J. Quant. Spectrosc. Radiat. Transfer* **2007**, *103*, 394.
[24] H. X. Xu, *Phys. Lett. A* **2003**, *312*, 411.
[25] H. X. Xu, E. J. Bjerneld, M. Kall, L. Borjesson, *Phys. Rev. Lett.* **1999**, *83*, 4357.
[26] S. E. A. Gratton, S. S. Williams, M. E. Napier, P. D. Pohlhaus, Z. Zhou, K. B. Wiles, B. W. Maynor, C. Shen, T. Olafsen, E. T. Samulski, J. M. DeSimone, *Acc. Chem. Res.* **2008**, *41*, 1685.
[27] J. P. Rolland, E. C. Hagberg, G. M. Denison, K. R. Carter, J. M. De Simone, *Angew. Chem. Int. Edit.* **2004**, *43*, 5796.
[28] Y. Cui, M. T. Bjork, J. A. Liddle, C. Sonnichsen, B. Boussert, A. P. Alivisatos, *Nano Lett.* **2004**, *4*, 1093.
[29] L. J. Wan, M. Terashima, H. Noda, M. Osawa, *J. Phys. Chem. A* **2000**, *104*, 3563.
[30] C. M. Whelan, M. R. Smyth, C. J. Barnes, *Langmuir* **1999**, *15*, 116.
[31] Z. B. Wang, B. S. Luk'yanchuk, W. Guo, S. P. Edwardson, D. J. Whitehead, L. Li, Z. Liu, K. G. Watkins, *J. Chem. Phys.* **2008**, *128*(9), 094705.